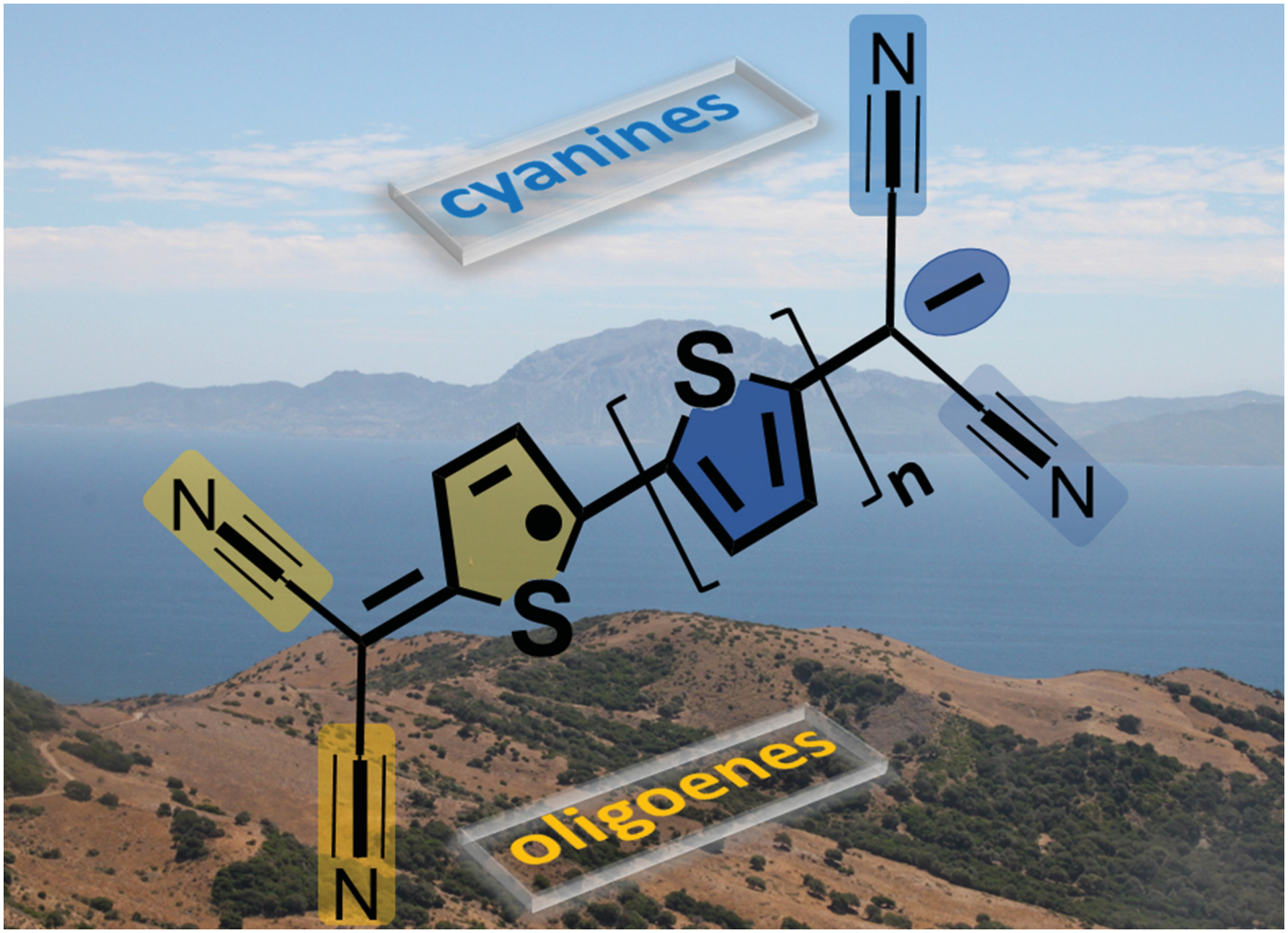

Showcasing research from Professor Casado's laboratory, Faculty of Science, University of Málaga, Málaga, Spain.

Oligoene and cyanine features of tetracyano quinoidal oligothiophenes

Transiting between the neutral and charged species of tetracyanoquinoidal oligothiophenes allows us to move from the properties of even-electron oligoenes and odd-electron cyanines, respectively. The redox tuning of the optical and structural features is uncovered here by spectroscopic analysis combined with electrochemistry. The cover picture shows how these π-conjugated quinoidal oligothiophenes bridge two different worlds, those of oligoenes and cyanines. For the last 20 years, we have been studying the unique structures of quinoidal molecules now revealing the underlying connection with the cyanine's world.

As featured in:

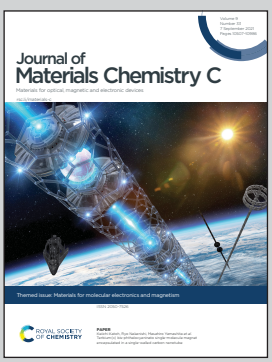

See Juan Casado *et al.*, *J. Mater. Chem. C*, 2021, **9**, 10727.

ROYAL SOCIETY OF CHEMISTRY

rsc.li/materials-c

Registered charity number: 207890

Journal of Materials Chemistry C

ROYAL SOCIETY OF CHEMISTRY

PAPER

View Article Online
View Journal | View Issue

Cite this: J. Mater. Chem. C, 2021, 9, 10727

Oligoene and cyanine features of tetracyano quinoidal oligothiophenes†

Sergio Moles Quintero,[a] José Luis Zafra,[a] Keitaro Yamamoto,[b] Yoshio Aso,[b] Yutaka Ie[bc] and Juan Casado*[a]

This paper interprets a palette of spectroscopic data on tetracyano thienoquinoidal molecules of different sizes oriented towards the elucidation of their electronic behavior and other aspects of interest in materials chemistry. It also provides a contextualization of these properties between those of even oligoenes (carotene-like) and those of odd cyanines as a function of the reduction state. A complete UV-Vis-NIR electronic absorption, fluorescence emission and infrared spectroscopic study in part helped by quantum chemical calculations in the framework of the DFT theory has been carried out. The study encompasses the neutral and charged states. The optical properties of these compounds in the neutral state are controlled by the competition of bright (electric dipole–dipole allowed) and dark (electric dipole–dipole forbidden) singlet excited states. In the anionic state, the trimeric compounds disclose behaviors compatible with being either charge localized or delocalized mixed valence systems. Interestingly, we show the π-dimerization of a radical anion of a thienoquinoidal compound forming a π-dimer dianion as a manifestation of the delocalization of the charge in the charged monomer. The hexamer compound in the neutral state discloses incipient diradical character which permits the detection of a NIR emission band from the dark state at energies well below 1 eV. As thiophene benzo-annulation minimizes the diradical character, it forces the confinement of the charge in the vicinity of the terminal dicyanomethylene groups in the dianion. The oxidized species of the compounds have been also analyzed as models of charge localization states. The competition between doublet and quartet high spin states in the radical cations has been explored with the objective of visualizing potential molecules able to produce SOMO–HOMO energy inversion. This paper adds an interesting perspective of the electronic structure of quinoidal molecules with respect to their interest in the field of organic electronics.

Received 29th March 2021,
Accepted 19th May 2021

DOI: 10.1039/d1tc01436f

rsc.li/materials-c

I. Introduction

Aromatic oligothiophenes,[1] AOTs in Scheme 1, are well-known in the field of organic electronics, with hexathiophene[2] being, together with pentacene,[3] one of the first organic π-conjugated compounds used as electrically active semiconductors in organic field-effect transistor (OFET) devices. These demonstrated to be p-type semiconductors[4] as expected for organic materials with an electron rich nature which prefer to stabilize and conduct positive charges (*i.e.*, being oxidized). Aromatic hexathiophene can be viewed as a *cis–trans* oligoene with 12 olefins where the cis conformation is fixed within the thiophene ring (Scheme 1). However, the aromatic character of thiophene makes these oligothiophenes deviate from the behavior of oligoenes, a detrimental aspect regarding the modulation of some properties such as π-electron delocalization and electronic and photonic properties based on it. Medium-long oligoenes are characterized by a first singlet excited state of dark nature[5] (forbidden by the dipole–dipole electric selection rules) which promotes two-photon absorption activity and, parallelly, fully quenches the molecular fluorescence. The presence of this dark excited state is also beneficial for applications such as

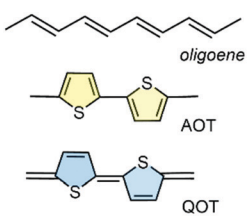

Scheme 1 Examples of the chemical structures of oligoenes (with four olefins), aromatic oligothiophenes (AOTs, bithiophene), and quinoidal oligothiophenes (QOTs, quinoidal bithiophene).

[a] Department of Physical Chemistry, University of Malaga, Campus de Teatinos s/n, 29071 Malaga, Spain. E-mail: casado@uma.es
[b] The Institute of Scientific and Industrial Research (ISIR), Osaka University, 8-1 Mihogaoka, Ibaraki, Osaka 567-0047, Japan
[c] Innovative Catalysis Science Division, Institute for Open and Transdisciplinary Research Initiatives (OTRI), Osaka University, 2-1 Yamadaoka, Suita, Osaka 565-0871, Japan

† Electronic supplementary information (ESI) available. See DOI: 10.1039/d1tc01436f

in singlet-exciton fission[6] because it is a precursor of the two entangled triplet states.[7]

Quinoidal oligothiophenes,[8–11] QOTs in Scheme 1, revert this situation. The extension of the electron wavefunction into the exocyclic bonds between the thiophenes disrupts its localization in the five membered rings by aromaticity. As a result, QOTs gain more oligoene-like character than their aromatic parents, thus recovering some of the beneficial properties of the carotenoid-like systems, such as the stabilization of the dark singlet excited state as the first energy lying singlet; in fact, this has enabled the appearance of intramolecular singlet exciton fission in one of the members of the QOTs.[12–14] The efficient inter-annular extension of π-electron delocalization in QOTs also gives rise to the appearance of the electronic absorption bands well displaced into the Vis-NIR region, indicating them to be NIR absorbing molecules. These optical properties of QOTs are accompanied by rich electrochemical properties in the cyclic voltammetry experiments showing reduction potentials at relatively low values and, in the case of the long oligomers, even reversible oxidations conferring amphoteric redox behavior.[15,16] This rich redox activity of QOTs has been exploited in organic field effect transistors with high electron mobility and ambipolar behavior in OFET devices.[17,18] More recently, tetracyanoquinoidal oligothiophenes have been studied by treatment with an electron donor to produce n-doped substrates which have been demonstrated to be efficient conductors for thermoelectric devices.[19]

AOTs with as many as 96 thiophenes[20] have been prepared. The longest QOTs, however, are hexamers.[8,16] These known hexamers are formed by dicyanomethylene encapsulation of the quinoidal core, a substitution that further contributes to the extension of π-electron delocalization, to the outstanding electron acceptor properties and to the intense Vis-NIR absorption. QOTs have been distinctively studied in recent years as stable diradicaloids.[8,16] This is based on the tendency to recover the aromaticity of the non-aromatic rings in the neutral state which for a certain molecular length (number of thiophenes) is able to stabilize the homolytic rupture of one double bond forming an open-shell diradicaloid.[8,16] Given the balance between aromaticity energy gain and the energy required to break a double bond, QOT diradicals are formed starting from the pentamer with the tetramer being in the borderline of the quinoidal → aromatic transition. Diradicaloids have appeared in the field of organic electronics given their promise to act as spintronic substrates based on their very low energy lying thermally accessible high spin triplet states which can act as spin polarizers or spin filters of current.[21,22] Diradicaloids and diradicals have been also demonstrated to be good non-linear optical chromophores[23,24] with large two-photon cross sections and large third order molecular hyperpolarizability, *etc.*

To the best of our knowledge, only a few tetracyano thienoquinoidal hexamers have been prepared and studied.[8,16] After more than 15 years since the first studies of these systems, herein we present the study of the electronic properties of a new tetracyano thienoquinoidal hexamer (**B2-6TQ** in Fig. 1) in the light of new spectroscopic properties as well as in comparison with shorter tetracyanothienoquinoidal parent compounds (**3TQ**, **B-3TQ**, **B3-3TQ** and **2TQ** in Fig. 1). A study of the electronic and vibrational properties of the tetracyanoquinoidal hexamer in connection with its diradicaloid, oligoene-like, and electron-acceptor characters is proposed. For this hexamer, the possibility to display SOMO–HOMO energy level inversion is also explored. On the other hand, the smaller trimeric compounds are analyzed from the point of view of their mixed valence properties and in the context of the properties of cyanines.

II. Experimental and theoretical methods

The syntheses of the benzothienoquinoidal compounds, **3TQ**, **B-3TQ**, **B3-3TQ** and **B2-6TQ**, have been recently reported.[25,26] On the other hand, the preparation and characterization of thienoquinoidal parent compound **2TQ** were published some years ago.[8] *In situ* infrared and UV-Vis-NIR spectroelectrochemical studies were conducted on a VERTEX 70 FT-IR spectrometer and on a Varian Cary 5000 UV-Vis-NIR spectrophotometer, respectively. A C3 epsilon potentiostat from BASi was used for the electrolysis using a thin layer cell from a demountable omni cell from Specac. In this cell a three electrode system was coupled to conduct *in situ* spectroelectrochemistry. A Pt gauze was used as the working

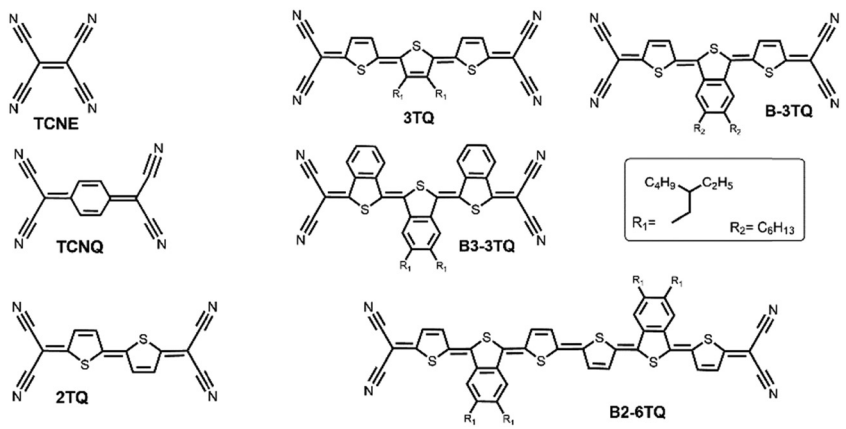

Fig. 1 Chemical structures of the QOTs studied and those of the known **TCNE**, **TCNQ** and **2TQ** used as reference compounds.

Table 1 Cyclic voltammetry (in volts) data for the first oxidation and reduction steps together with the corresponding energy levels (in eV) of the studied compounds. Values taken from ref. 25 and 26. (a) and (b) Waves corresponding to 2 and 1 electron processes, respectively

	3TQ[26]	B-3TQ[26]	B3-3TQ[26]	B2-6TQ[25]
$E^1_{1/2}$ (red)	−0.58[a]	−0.74[a]	−1.02[a]	−0.54[a]
E (LUMO)	−4.23	−4.06	−3.78	−4.26
$E^1_{1/2}$ (oxd)	0.81[b]	0.86[b]	0.81[b]	0.08[b]
E (HOMO)	−5.61	−5.66	−5.61	−4.88

electrode, a Pt wire was used as the counter electrode, and an Ag wire was used as the pseudo-reference electrode. The corresponding cyclic voltammetry data and related energy levels are shown in Table 1 and are taken from ref. 25 and 26. The spectra were collected using constant potential electrolysis and the potentials were changed in intervals of 10 mV. The electrochemical medium used was 0.1 M tetrabutyl ammonium hexafluorophosphate, Bu_4NPF_6, in fresh distilled dichloromethane, at room temperature with a sample concentration of 10^{-3} M. Low temperature absorption and emission measurements were carried out in a cryostat OPTISTAT cell from Oxford Instruments.

Emission fluorescence spectra were obtained using a JASCO V-570 spectrometer. The measurements were carried out in degassed/anhydrous dichloromethane. All solvents used were of spectroscopic grade purchased from Aldrich. The emission spectra in the NIR region were obtained either by using a Bruker Senterra Raman spectrometer equipped with a microscope with excitation up to 785 nm by averaging spectra during 10 min with a resolution of 3–5 cm^{-1} or by using a RAMII FT-Raman module of a VERTEX 70 FT-IR spectrometer with excitation at 1064 nm. The Raman and emission scattering radiation was collected in a back-scattering configuration with a standard spectral resolution of 4 cm^{-1}. 500 scans were averaged for each spectrum.

Quantum chemical calculations were done with the Gaussian16 suite of programs.[27] Molecular geometry optimizations were performed with the B3LYP functional and the 6-31G** standard basis set.[28,29] Energy optimizations were performed by allowing all geometric parameters to vary independently. For the analysis of the open-shell diradicals, the broken-symmetry approximation in the unrestricted DFT methodology (UDFT) was assumed. The singlet–triplet energy gaps were calculated as the energy difference between those of the optimized geometries of the singlet-open shell (broken symmetry) and triplet electronic states. The UDFT methodology was also used for the theoretical study of the energies and geometries of monoradical systems. Vertical transition energies were computed with the time-dependent version of DFT (TDDFT) at the same level of theory.[30,31] Some additional basic theoretical data such as the energy values of the frontier molecular orbitals are available in the corresponding articles where the molecules were reported.

III. Results and discussion

III.1. Electronic structure of the neutral compounds

Fig. 2 displays the electronic absorption spectra of the three quinoidal trimers, **3TQ**, **B-3TQ** and **B3-3TQ**. In **3TQ** the main

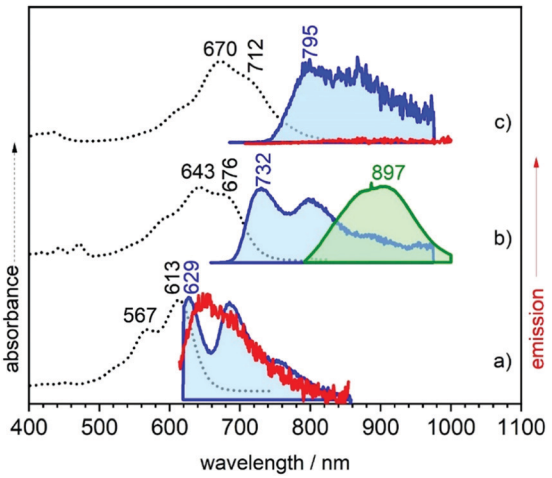

Fig. 2 UV-Vis-NIR absorption (black dotted lines) and emission (red and green lines at 298 K and blue lines at 80 K) spectra of (a) **B3-3TQ**, (b) **B-3TQ**, and (c) **3TQ**.

absorption band appears at 670 nm, as in other reported quinoidal trimers. This band blue-shifts upon incorporation of one and three benzothiophene units up to 643 nm in **B-3TQ** and to 613 nm in **B3-3TQ**. These bands correspond to the respective HOMO → LUMO one electron transitions according to TD-DFT calculations which predict them at 624 nm in **3TQ**, at 599 nm in **B-3TQ** and 568 nm in **B3-3TQ** in nice agreement with the experimental data and trends (Fig. S1, ESI†). This wavelength maxima behavior is a consequence of the destabilization of the LUMO (Fig. S2, ESI†) on **3TQ** → **B-3TQ** → **B3-3TQ** due to the increasing number of nodes in the wavefunction upon inclusion of lateral benzenes (*i.e.*, between the thiophene carbon atoms and those of the benzenoid rings). This is nicely reflected in the electrochemical reduction potentials of the three compounds which evolve to more negative values of −0.58 V in **3TQ**, −0.74 V in **B-3TQ** and −1.02 V in **B3-3TQ**.[25,26] Interestingly, despite the cathodic displacement of the potentials, the reduction waves all correspond to the transference of two electrons each suggesting that the destabilization of the LUMO is accompanied by a progressive localization of the extra charge in the reduced species in two separated domains. This would make the electron transfer of two electrons happen at similar potentials (not distinguished in the cyclic voltammetry experiment). Conversely to the cyclic voltammetry experiment, in the spectroelectrochemical cell during reduction, we will describe below the distinctive and subsequent formation of a radical anion and of a dianion in the three smaller quinoidals. On the other hand, the HOMO energy of the three trimeric compounds (Fig. S2, ESI†) is scarcely affected in the series owing to the non-bonding character of the connecting atoms between those of the thiophenes and of the benzenes explaining the very similar oxidation potentials for the generation of their radical cations.[25,26] The overall result is an enlargement of the HOMO–LUMO gap and of the optical gap upon increasing numbers of benzothiophenes.

The emission properties of the studied compounds have been analyzed upon excitation of the main absorption bands. The three quinoidal trimers show very weak or no emission at

room temperature in the range up to 1100 nm. In this regard, to complement these data, Fig. 2 also shows the spectra at 80 K. There are significant changes from molecule to molecule in the low temperature spectra: whereas **B3-3TQ** displays an emission associated with the optically pumped excitation band with a small Stokes shift (*i.e.*, 415 cm^{-1}), **B-3TQ** shows an emission band with a larger Stokes shift (*i.e.*, 1130 cm^{-1}) and, finally, **3TQ** exhibits a broad band (not resolved at room temperature) featuring a Stokes shift of $\approx$1600 cm^{-1}. Interestingly, upon excitation at 785 nm of the low energy part of the intense absorption of **B-3TQ**, a new emission feature is detected at room temperature that is not detected upon excitation on the peak maxima (643/676 nm) of the intense band under the same temperature conditions. This new band shows a similar shape to the main absorption band with a maximum at 897 nm thus representing a very large Stokes shift of $>$4500 cm^{-1}. This makes us likely to ascribe this emission to a radiative process from a different excited electronic state which is lower in energy compared to that linked with the main band of the absorption spectrum. The low temperature spectra of **B3-3TQ** and **B-3TQ** clearly disclose vibronic structures related with the increment of torsional mobility in the excited state upon partial relaxing of the planarity between the thiophene rings imparted by the quinoidal shape in the ground electronic state.

It is known for quinoidal compounds that there is a dark singlet excited state[12,13] (*i.e.*, non-allowed by the electric dipole selection rules, denoted as S_2 in Fig. 3) close in energy to the optical state (*i.e.*, bright state, denoted as S_1 in Fig. 3) that must be considered to explain their photophysical properties. This excited state distribution in quinoidal compounds is very similar to that described in oligoenes and carotenoid-like compounds.[5] In **B3-3TQ**, the situation is that the S_1 is lower in energy than S_2 by which we detect the emission only from S_1, or $S_1 \rightarrow S_0$ at 629 nm, thus accounting for its small Stokes shift. In **B-3TQ**, the situation is that the energies of the S_1 and S_2 are very close, consequently promoting $S_1 \rightarrow S_2$ conversion through a conical intersection which has been described in similar quinoidal compounds;[13] the overall result in **B-3TQ** is the detection of the two $S_1 \rightarrow S_0$ and $S_2 \rightarrow S_0$ emissions (a wrong very large Stokes shift is found if we consider the absorption by the S_1 and the emission from the S_2). Finally, in **3TQ**, the situation is that $S_1 \rightarrow S_2$ is apparently blocked, by which none of them are detected at room temperature due to the smallest gaps (the $S_1 \rightarrow S_0$ is weakly detected at low temperature). TD-DFT calculations predict the bright singlet excited state always as the $S_0 \rightarrow S_1$ absorption with the $S_0 \rightarrow S_2$ excitation lying always higher in energy for the three compounds. It is well known, however, that the relative disposition of these two excited states is strongly dependent on electron correlation which is not fully considered in our simple TD-DFT approach; thus, we are confident that if these correlation effects would be taken into account in calculations, such as already reported for a homologue **2TQ** quinoidal compound,[8,16] the most likely evolution of the energy of the S_2 state in the three compounds is such as that in Fig. 3 (note that high level theoretical calculations are beyond the objective of the present work).

III.2. Electronic structure of the charged species in the context of mixed valence behavior

As already mentioned, in the spectroelectrochemical experiment, the spectra of the anion radicals and of the dianions are distinguished. Given the electron withdrawing character of the cyano groups, these drain the added negative charge; the point is whether the charge in the radical anion is preferentially stabilized in one of the dicyanomethylenes or stabilized by semi-contributions of the two and by the bridge. In the framework of the Robin–Day classification[32] of mixed valence systems,[33] these two situations correspond to a charge localized class II mixed valence system and to a class III full delocalized mixed valence system, respectively. Recently, the interesting cases of mixed valence systems that behave in the frontier between class II and class III transiting between them depending on the external stimuli has also been established.[34] The starting point in this discussion is the case of the radical anions of the reference compounds **TCNE** and **TCNQ** (Fig. 1), which have been described as class III mixed valence systems with full charge delocalization between the two respective dicyanomethylenes.[35] In comparison with these, the discussion of the electronic absorption and infrared spectra of the charged species of **3TQ**, **B-3TQ** and **B3-3TQ** is presented.

III.2.1 UV-Vis-NIR electronic absorption spectra of charged species. The UV-Vis-NIR electronic absorption spectra of the radical anions of these trimers are disclosed in Fig. 4 and Fig. S3 (ESI†). The radical anion of **3TQ** displays the typical

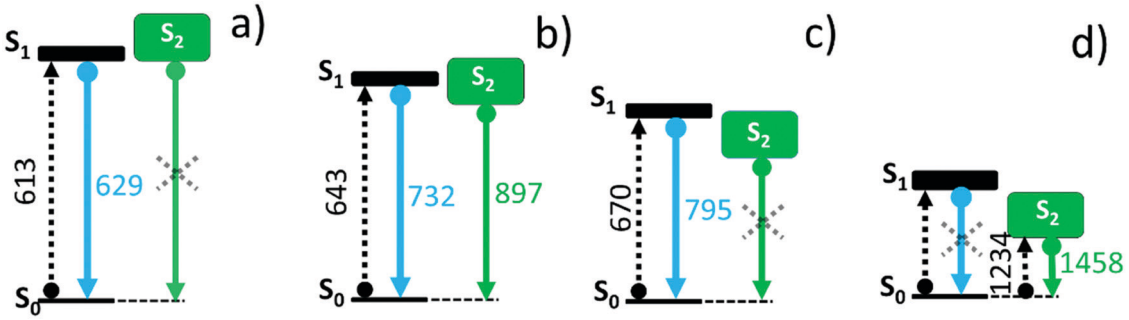

Fig. 3 Qualitative excited state energy ordering of the bright (S_1) and dark (S_2) states of the studied compounds: (a) **B3-3TQ**, (b) **B-3TQ**, (c) **3TQ** and (d) **B2-6TQ**. The broken arrows denote the absorption/excitation peaks and the solid arrows represent the emission either from the bright state (blue) or from the bark state (green).

aspect of the absorption spectra of charged monoradical[36,37] molecules of π-conjugated systems with two main bands, one in the visible region of the spectrum at 675 nm and another broad band with vibronic structure in the NIR region with maxima at 1217 nm (shoulder at 1359 nm), both spaced by 859 cm^{-1}. On the other hand, the spectral profile of the UV-Vis-NIR absorption spectrum of the radical anion of **B3-3TQ** displays, compared to the anion of **3TQ**, a very different profile composed of a much weaker band at 954 nm together with one very weak and broad, exempted of vibronic structure, at 1692 nm. The UV-Vis-NIR absorption spectral pattern of the anion of **B-3TQ** displays further differences relative to its parents with a pattern of two bands at 636 nm and the strongest one of three components at 937 nm all enclosed by two vibrational progressions of 2455 cm^{-1} and 859 cm^{-1}. The former vibrational spacing of **B-3TQ** is closer to the wavenumber of the C≡N stretching mode already revealing the intervention of the terminal cyano groups in this excitation, an effect absent in the spectrum of the **3TQ** anion (*i.e.*, one vibronic progression of 859 cm^{-1}). The weakness of the bands of the anion radical of **B3-3TQ** precludes the evaluation of the vibronic structure.

TD-DFT quantum chemical calculations were carried out for the three radical anions. For that of **3TQ**, theory predicts two main excitations at 675 nm correlated with the experimental one at 660 nm and another transition at 1192 nm corresponding with the experimental bands at 1217/1359 cm^{-1}. Though calculations of the neutral compounds and of the radical anion of **3TQ** reproduce well the experiments, the same level calculations in the other two radical anions do not work well. The UV-Vis-NIR absorption spectra of the dianions of the three thienoquinoidal trimers display one main band which contrarily to the case of the radical anions red-shifts from **3TQ** (*i.e.*, at 445 nm), to **B-3TQ** (*i.e.*, at 585 nm), and to **B3-3TQ** (*i.e.*, at 618 nm).

The three compounds can be also reversibly oxidized to the radical cations whose UV-Vis-NIR absorption spectra are collected also in Fig. 4 and Fig. S4 (ESI†). The spectra of the three cationic species share similar patterns which consist of two features: (i) moderate/strong/weak visible bands at 675, 722 and 766 nm in **3TQ**, **B-3TQ** and **B3-3TQ**, respectively, which (ii) are accompanied in the three cases by very weak NIR absorption at 1201/1418 (*i.e.*, spaced by 1274 cm^{-1}), 1245/1501 nm (*i.e.*, spaced by 1370 cm^{-1}), and 1075/1247 nm (*i.e.*, spaced by 1283 cm^{-1}) in the three compounds, respectively. The similar energy spacing of the three progressions reveals the confinement of the charge in similar molecular parts. These spectra typically correspond to species with highly localized charge defects, that is, extraction of the charge in the parent neutral compound takes place far apart of the electron withdrawing cyano groups, very likely in the

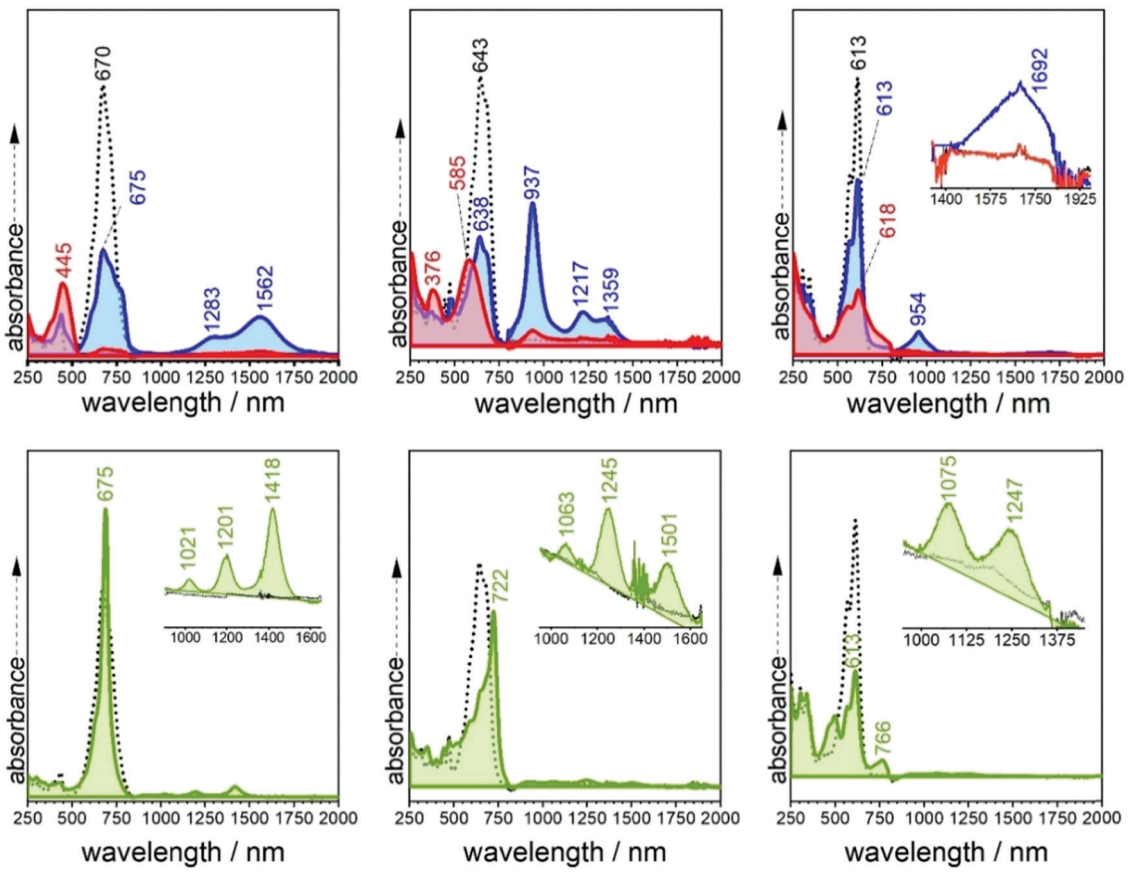

Fig. 4 Top (bottom): UV-Vis-NIR electronic absorption spectra taken during the spectroelectrochemical reduction (oxidation) in 0.1 M $TBPF_6$ in CH_2Cl_2 at room temperature of **3TQ** (left), **B-3TQ** (middle) and **B3-3TQ** (right). Neutral (broken lines), radical anions (blue shaded), dianions (red shaded) and radical cations (green shaded).

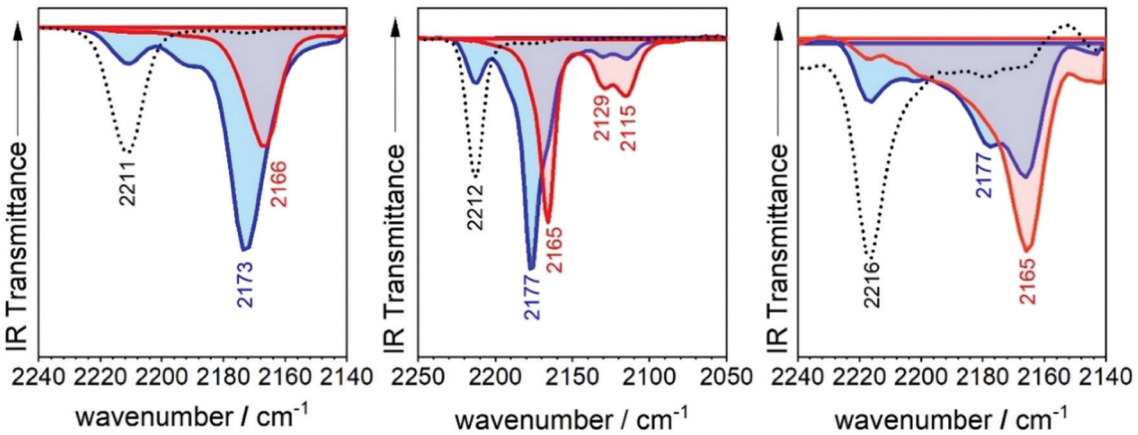

Fig. 5 Infrared spectra taken during the spectroelectrochemical reduction in 0.1 M $TBPF_6$ in CH_2Cl_2 at room temperature of **3TQ** (left), **B-3TQ** (middle) and **B3-3TQ** (right). Neutral (broken lines), radical anions (blue shaded) and dianions (red shaded).

molecular center around the electron rich sulfur atom(s) of the central thiophene(s). The discussion of these features in the cationic absorption spectra allows us to compare radical anions and radical cations of **B3-3TQ:** both monovalent species have a common spectral fingerprint related with the presence of very weak absorption NIR bands due to the existence in both of localized charged defects. The difference between the two is that in the anion the charge confinement is on/around the cyano moieties while for the cation the charge is preferentially accommodated closer to the central thiophenes.

Contrary to the cases of the benzothiophene quinoidals, in the anion radical of **3TQ** there are indications that suggest that this can be assigned to a delocalized class III mixed valence species. These are: (i) the UV-Vis-NIR absorption spectra of the radical anion and dianion of the homologue **2TQ** have been obtained (Fig. S5, ESI†). The cyclic voltammetry of **2TQ**[38] shows two well resolved and distinctive one-electron reductions due to the univocal formation of an anion radical followed by a dianion. The radical anion discloses an absorption spectrum with bands at 629 and 1062 nm (with a shoulder at 922 nm spaced by 1430 cm^{-1}), and thus, with a very similar pattern to that of the radical anion of **3TQ** in line with both radical anions sharing the same class III mixed valence property. (ii) Overall, the large differences in the shapes of the radical anion spectra of the three trimers suggest these to possess different electron distributions. (iii) Finally, the existence of a cyano based vibronic progression in the radical anion of **B-3TQ** further supports this to be of localized character around these groups.

III.2.2 Infrared spectra of charged species. The infrared absorption spectra of the radical anions of the trimer quinoidal have been also recorded during the electrochemical reduction and are shown in Fig. 5 and Fig. S6 (ESI†) together with those of the electrochemically generated dianions.

The infrared spectrum of **3TQ** in the anion radical state is characterized by a main band due to the C≡N stretching vibration at 2173 cm^{-1} which evolves from that at 2211 cm^{-1} in the neutral species. Subsequent reduction of this to the dianion gives rise to a further wavenumber downshift to 2166 cm^{-1}. The wavenumber downshift of the C≡N stretching infrared band, $\Delta\nu$(CN), is a result of the antibonding character of the LUMO orbitals in the cyano groups so that their occupation upon reduction enlarges the C≡N distance and decreases the wavenumber of the associated stretching band. This process is progressive up to 2166 cm^{-1} on going from the radical anion to the anion of **3TQ** due to the double occupancy of the initial LUMO. Reduction of **B-3TQ** also produces a change from 2212 cm^{-1} in the neutral species to 2177 cm^{-1} in the radical anion and 2165 cm^{-1} in the dianion, whereas in **B3-3TQ**, the ν(CN) infrared band is at 2216 cm^{-1} which moves up to 2177 cm^{-1} in the radical anion and to 2165 cm^{-1} in the dianion. The evolution of the wavenumber values in all neutrals, radical anions and dianions of all tetracyano compounds in this work is presented in Fig. 6. The $\Delta\nu$(CN) is a very sensitive measure of the charge excess installed in the cyano groups upon reduction[39] with the prototypical example of tetracyanoethylene (*i.e.*, **TCNE** in Fig. 1) and tetracyanoquinodimethane (*i.e.*, **TCNQ**) whose $\Delta\nu$(CN) is also shown in Fig. 6. For the smaller **TCNE**, the $\Delta\nu$(CN) values from the neutral to the anion radical and from this to the dianion are similar, spectroscopic changes in line

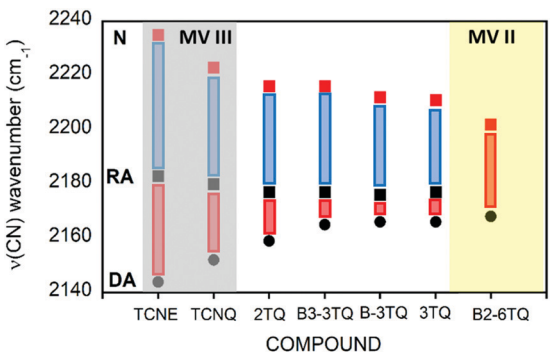

Fig. 6 Representation of the values of the ν(CN) bands from the infrared spectra of the neutrals (red squares), radical anions (black squares) and dianions (black circles) of the tetracyano compounds studied in this work. The blue and red bars display the $\Delta\nu$(CN) values in the two reduction steps.

with the charge of the radical anion of **TCNE** to be fully delocalized among the four cyano groups (*i.e.*, approx. 1/4 of the charge on each cyano in the anion). In its dianion, driven by electrostatic repulsion, one charge is on each dicyanomethylene group (*i.e.*, 1/2 of charge on each cyano). As a result, the addition of one electron on neutral → anion and on anion → dianion generates similar changes in the ν(CN) bands (each cyano group doubles its charge in each reduction step). For **TCNQ**, the $\Delta\nu$(CN) from the neutral (at 2223 cm^{-1}) to the anion radical (at 2180 cm^{-1}), by 43 cm^{-1}, is greater than that from the anion to the dianion (at 2152 cm^{-1}), by 28 cm^{-1}. The larger shift in the neutral → anion step might reveal that the distribution of the charge in the **TCNQ** anion differs from that of the anion radical of **TCNE**. Furthermore, the infrared spectra of the anionic species of **2TQ** have been obtained and shown in Fig. S5 (ESI†) which, for the radical anion, display a main ν(CN) band at 2177 cm^{-1} (neutral one at 2216 cm^{-1}) disclosing a $\Delta\nu$(CN) in this first step of 39 cm^{-1}. Going to the dianion, the ν(CN) band of **2TQ** moves to 2159 cm^{-1} yielding a $\Delta\nu$(CN) value of 18 cm^{-1} reinforcing the dissymmetry of the electron distribution in the two reduction steps.

The radical anions of the thienoquinoidal trimers display (i) very similar $\Delta\nu$(CN) shifts from the neutral to the anion: 38 cm^{-1} in **3TQ**, 35 cm^{-1} in **B-3TQ** and 39 cm^{-1} in **B3-3TQ** indicating similar affectation of the CN moieties upon single charging; and (ii) from the anion to the dianion, the shifts are much smaller than in the previous reduction step with $\Delta\nu$(CN) of 7 cm^{-1} in **3TQ** and 12 cm^{-1} in **B-3TQ** and **B3-3TQ**. From the point of view of the $\Delta\nu$(CN) values, the way to conciliate these findings in the thienoquinoidal compounds is assuming a transition from class III full delocalized to class II localized mixed valence species. A class II localized situation would confine the charge around one of the dicyanomethylene terminals by which the $\Delta\nu$(CN) of the first reduction step would be similar in all thienoquinoidal cases irrespective of the size/nature of the bridge. In addition, from such localized state post-reduction to the dianion would impart smaller variations. Hence, according to the infrared spectra, the radical anions of **B-3TQ** and **B3-3TQ** are closer to the class II species with confinement of the charge on the dicyano groups. In the case of **3TQ**, the infrared data discussion places this as a class II compound whereas the interpretation of the UV-Vis-NIR absorption features revealed this as class III. As a result, **3TQ** could behave more in the transition region between classes III and II.

A tentative reason for the stabilization of the class II form at the expense of the class III structure in the anions of **B-3TQ** and **B3-3TQ** can be related with the significant reduction of the bond length alternation (*i.e.*, BLA) pattern between the consecutive CC bonds of the π-conjugated core on passing from the neutral to the radical anions. The proximity of the structure to a vanishing BLA prepares this to undergo pseudo Jahn–Teller (p-JT) distortion towards an asymmetric structure with increasing BLA. This p-JT effect is often acting together with solvation effects meaning the formation of a structure with the solvated charge mainly around one of the two dicyanomethylene parts or localized class II form, as described in Scheme 2. Also in agreement with this vision is the two-electron transfer process

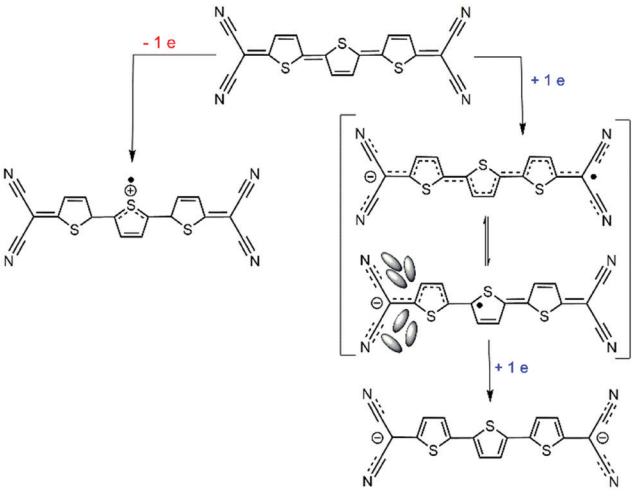

Scheme 2 Representation of the evolution of the **3TQ** structure upon reduction/oxidation. In the radical anion, specific solvation (solvent molecules are denoted as shaded discs) of the charge and p-JT might justify the existence of an equilibrium of the full delocalized and localized forms.

observed in the cyclic voltammetry experiment of the thienoquinoidal trimers which reveals the introduction of two electrons at potentials below the electrochemical threshold in line with each one somehow entering in independent moieties.

III.2.3 Radical anions of thienoquinoidals *vs.* cyanines. We discussed the common behavior of neutral tetracyano substituted thienoquinoidal compounds compared with those of oligoenes both being based on systems with an even number of electrons in the π box. Upon single charging of the quinoidal compounds, these convert into molecules with an odd number of π-electrons what inspires a comparison with polymethines and with their charged analogues, cyanines.[40,41] Cyanines in Scheme 3 are conjugated cations formed by two nitrogen atoms

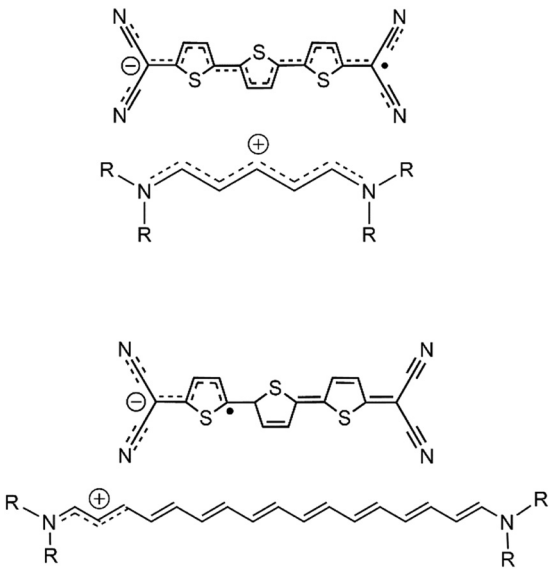

Scheme 3 Comparison between delocalized/localized cyanines and delocalized/localized forms of the radical anion of **3TQ**.

connected to the terminal parts of a polymethine chain with one of the nitrogens in a quaternary state. Cyanines, as a function of the size, can be divided into two classes, full delocalized cyanines in which the cation charge resonates/delocalizes over the whole polymethine chain, which corresponds to the case of the shorter members, and long cyanines that feature localization of the charge in one of the two terminal parts around one of the nitrogens. As a result, going from the shorter to the longer cyanines, a delocalized to localized transition takes place which is referred to as the cyanine limit.[42] In cyanines, the reasons for the symmetry breaking from the delocalized to the localized state are twofold: (i) ion-pairing with the counter-anion and solvation of the itinerant cation that favors the localized state; and (ii) the small BLA in the delocalized state that is energetically stabilized by undergoing p-JT effects towards a distorted structure. The net result of these effects is the stabilization of a distorted structure by symmetry breaking in longer cyanines. Among the experimental pieces of evidence that reveal the symmetry breaking effect in cyanines is the alteration of the optical spectra from intense well-defined sharp NIR electronic absorption bands in the delocalized state (small cyanines) towards blue-shifted broad and less intense bands in the localized state (long cyanines).

The data discussed in the radical anions of the tetracyano thienoquinoidal trimers establish a parallelism with the behavior of cyanines. The similitude between the radical anions of the tetracyano quinoidal compounds and the cyanines are (i) both disclose an odd number of π-electrons in conjugation; (ii) whereas the amine/imine pair of the nitrogen functionalization produces the transmission of the cation along the polymethine path, in the quinoidal compounds, the cyano/imine character of the CN groups imparts the conjugation effect of the negative charge in the radical anions; and (iii) the absorption spectra evolve from intense well resolved NIR bands in the smaller bridge compounds (see the spectra of the radical anion of **2TQ** in Fig. S5, ESI† and **3TQ** in Fig. 3) towards broader less intense bands in the radical anions of the benzoannulated quinoid trimers. This comparison agrees with the existence of a transition between the delocalized and localized states in the radical anions of the quinoidal trimers, an evolution that will be completed in the case of the longer oligomer, such as the case of the tetracyano thienoquinoidal hexamer that will be discussed in Section III.2.5.

III.2.4 Low temperature UV-Vis-NIR spectra and π-dimerization of the radical anions. The way intermolecular aggregation processes take place in solids is of fundamental importance for the design of electroactive substrates and materials.[43] Among these phenomena, the formation of basic face-to-face dimers of charged π-conjugated molecules, or π-dimers,[44] has been historically important as the building blocks of models to account for electrical conduction in organic solids. Most of the studied π-dimers correspond to associations of cations due to the greater propensity of π-electron rich conjugated molecules to form these defects and stabilize them intermolecularly. One of the former studies of π-dimers of cations of π-conjugated molecules was carried out by the group of professor Larry L. Miller in the University of Minnesota describing the formation

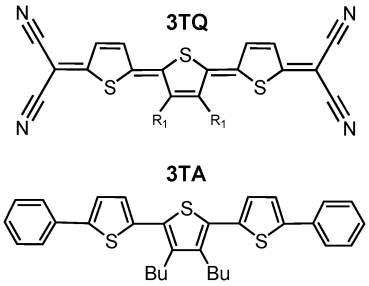

Scheme 4 Chemical structure of the quinoidal **3TQ** in comparison with that of its aromatic counterpart, **3TA** (Bu: *n*-butyl), a prototypical oligothiophene able to form π-dimeric dications.

of π-dimers of radical cations of oligothiophenes,[45–47] in particular, the π-dimer of the radical cation of a diphenyl aromatic terthiophene, **3TA** in Scheme 4. In contrast, the number of organic molecules able to stabilize negative charges is much smaller than that stabilizing cations and, of these,[48] only a few have been proven to form stable π-dimers of negative charges yielding diamagnetic π-dimer dianions.[49–51] Despite the large number of quinoidal oligothiophenes reported so far, no studies about the ability of these to form π-dimers of radical anions have been reported.

One way to explore the presence and formation of π-dimers is by addressing the evolution of the electronic absorption spectra in solution on cooling as the aggregation reaction is thermodynamically favored by reduction of the entropic term by lowering the temperature. In this situation, the spectroscopic fingerprint of the π-dimer formation should then appear, which, in the case of the terthiophene dication π-dimer of **3TA**,[47] is characterized by new bands at 1012 nm and 590 nm that grow up progressively on cooling at the expense of the 1106 nm and 654 nm features of the individual radical cations of **3TA** at room temperature.

The radical anion of **3TQ** has been obtained by chemical reduction and low temperature spectroscopic measurements of its solution carried out such as shown in Fig. 7. At room temperature, the spectrum of the radical anion of **3TQ** features 675 and 1570 nm bands. In the initial steps of the cooling, these bands

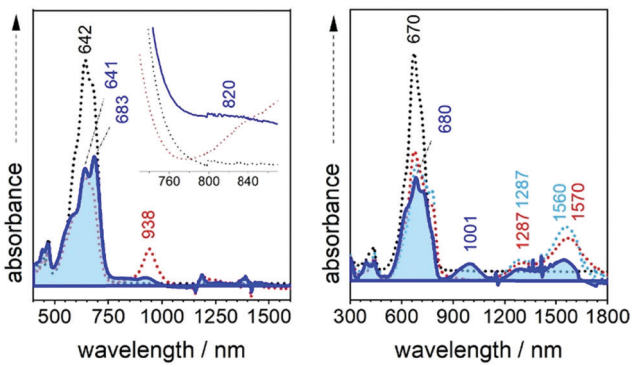

Fig. 7 UV-Vis-NIR absorption spectra of the radical anions of **B3-3TQ** (left) and of **3TQ** (right) from 298 K to 210 K (blue shaded spectrum) in CH_2Cl_2.

of the individual molecule increase their intensity up to 210 K upon which a new pair of bands at 680 nm and more notably at 1001 nm rises isosbestically. This behavior is very similar to that described for the radical cation of **3TA**[47] and the similitude of the wavelength position of the NIR bands of low temperature species of both the radical anion of **3TQ** (1001 nm) and the radical cation of **3TA** (1012 nm) is certainly indicative that similar species have been generated on cooling. This situation suggests the formation of a π-dimer dianion from two radical anions of **3TQ** which, for the first time, is described for the cathodic species of thienoquinoidal molecules. The same experiment has been carried out for the radical anion of **B-3TQ** in Fig. 7; upon cooling, its electronic absorption spectra evolve with some similarity to the case of **3TQ** with the intensification of a new band at 820 nm which emerges isosbestically from the band at 938 nm of the radical anion at room temperature. This might reveal that **B-3TQ** also shows propensity to form π-dimer dianions.

The formation of π-dimer dianions from the radical anions of the thienoquinoidal compounds is indicating that the charge in the individual ions is distributed over the whole π-conjugated skeleton which is the preferred form to accomplish efficient multi-bonding center coupling to stabilize the aggregated structure. This description is more consistent with a full delocalized class III mixed valence system rather than a class II in which the confinement of the charge would make the intermolecular interaction less favorable. This discussion for **3TQ** is in agreement with the description that its radical anion behaves in the class II/III mixed valence frontier and corroborates how external stimuli could move the charge in the direction of delocalization or confinement depending on the perturbation.

III.3. Electronic structure of tetracyanoquinoidal hexathiophene

Extension of the π-conjugated structure from thienoquinoidal trimers to a thienoquinoidal hexamer (*i.e.*, **B2-6TQ** in Fig. 1) introduces the stabilization of an open-shell diradical ground electronic state as previously reported for a similar quinoidal hexamer.[8,16]

In Fig. 8, DFT/UB3LYP/6-31G** calculations of the complete series of neutral tetracyano thienoquinoidal compounds are shown calculated either as closed or open-shell singlets. Two series consisting of unsubstituted quinoidal thiophenes (***n*TQ**) and all benzothienoquinoidals (**B*n*-*n*TQ**) from a monomer to heptamer (n = 1–7) have been calculated. We find that for the ***n*TQ** series starting from the pentamer the open-shell singlet diradical is the most stable situation for the ground electronic state with a very reduced singlet–triplet gap of <2 kcal mol^{-1}. Conversely, substitution of the thiophenes with benzene groups in benzothienoquinoidal units destabilizes the open-shell form and all the calculated systems become singlet closed-shell ground

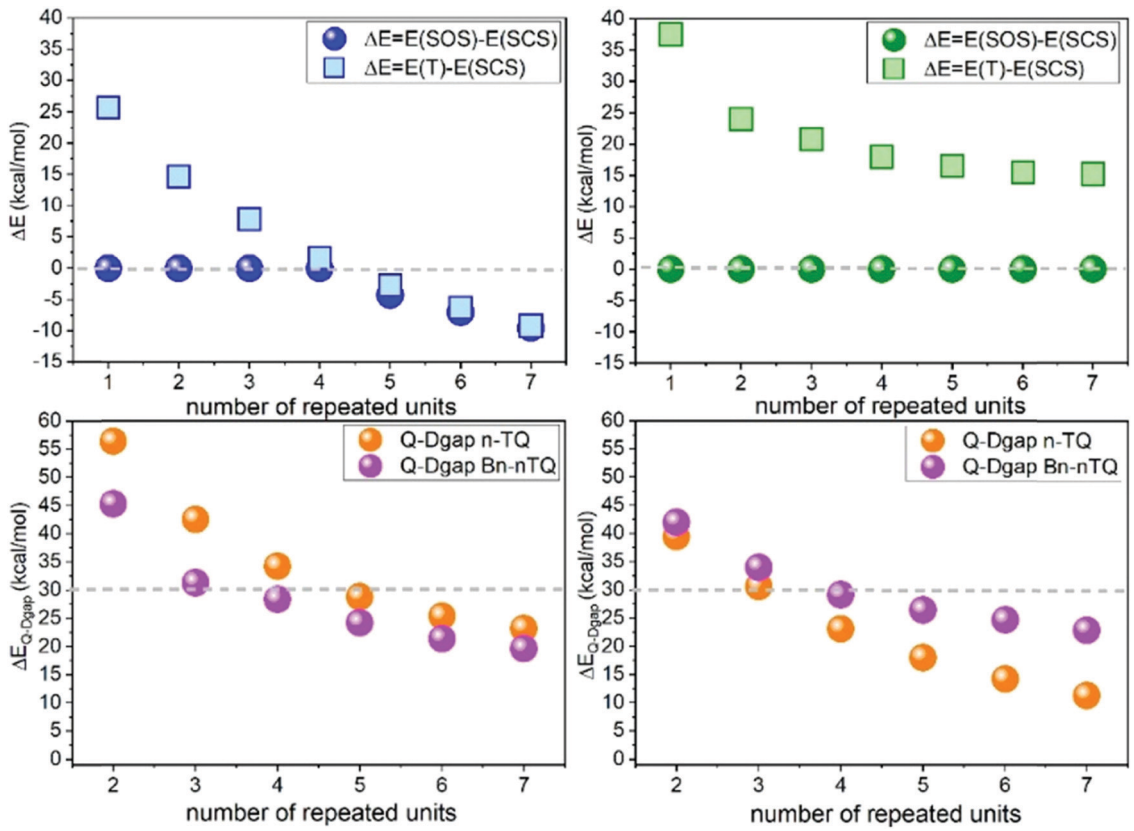

Fig. 8 Top: DFT/(*U*)B3LYP calculations of the energy differences (Δ*E*) between the singlet closed (SCS) or open-shell (SOS) ground electronic states and the first excited state triplets (T) in the ***n*TQ** (left) and **Bn-*n*TQ** (right) series. Bottom: DFT/UB3LYP calculations of the energy differences between the ground electronic state doublet (D) and first quarter excited state (Q) of the radical anions (left) and cations (right) of the same series.

electronic states. Within these two extremes, **B2-6TQ** should display a situation between the two hexamers. In particular, calculations for **B2-6TQ** disclose a theoretical singlet–triplet gap of 4.2 kcal mol^{-1} and a diradical index[52] y_0 = 0.142 (*i.e.*, y_0 varies from y_0 = 0 for closed-shell molecules to y_0 = 1 for completely formed diradicals) revealing an incipient diradical character for **B2-6TQ**. On the other hand, it is clear that all the above studied thienoquinoidal trimers disclose a closed-shell configuration in their ground electronic state.

The electronic absorption spectrum of **B2-6TQ** in Fig. 9 is constituted by a broad band with the peak maximum at 978 nm which is due to the electric dipole allowed $S_0 \rightarrow S_1$ excitation (as in the trimer compounds). This band displays a vibronic structure with shoulders at high and lower energies. However, by deconvolution (Table S1, ESI†), we obtain four components (Fig. 9) which compared with the pattern of three vibronic peaks on the trimers suggests that the deconvoluted peaks at 890, 974 and 1037 nm might belong to the $S_0 \rightarrow S_1$ band, whereas the additional peak red-shifted at 1207 nm might arise from the $S_0 \rightarrow S_2$ excitation described as a dark state in the previous sections. Contrarily to the other quinoidal compounds, this $S_0 \rightarrow S_2$ band emerges in the electronic absorption spectrum of **B2-6TQ** as a result of the diradical character imprinted in its ground electronic state. The appearance of this two-photon absorption band in the one photon optical spectrum as a weak feature is the confirmation of its open-shell diradical character.

In Fig. 9 the emission spectrum of **B2-6TQ** is also shown. By excitation at 785 nm of the strongest absorption band, no emission spectrum is recorded, a situation that is reversed by excitation at longer wavelengths in the $S_0 \rightarrow S_2$ band (blue shaded band in Fig. 9) which gives rise to a weak NIR emission with a maximum at 1458 nm assigned as the $S_2 \rightarrow S_0$ emission from the dark excited state. Therefore, a difference with the quinoidal trimers is that in **B2-6TQ** we detect the $S_0 \rightarrow S_2/S_2 \rightarrow S_0$ absorption/emission pair. As shown in Fig. 2, the larger energy difference between the S_2/S_1 excited states in **B2-6TQ** reduces internal conversion between the two; hence, the low energy emission only appears upon excitation on its own absorption band.

III.4. Electronic structure of the charged species of B2-6TQ

Similar to the quinoidal trimers, **B2-6TQ** displays a two-electron reduction wave. However, contrarily to the case of the smaller size homologues, in the spectroelectrochemical experiment, the spectra of radical anions could not be resolved neither in the UV-Vis-NIR nor in the infrared scanning, and only one species due to the dianion appears in the whole cathodic potential range. The electronic absorption spectrum of the formed dianion species in Fig. 10 displays a band with a maximum at 571 nm (no NIR bands) in line with the 583 nm band in the dianion of **B-3TQ**. In the infrared spectroelectrochemical experiment, the ν(CN) band of the dianion is recorded at 2168 cm^{-1} which directly evolves from the ν(CN) band in the neutral at 2202 cm^{-1} meaning a change, $\Delta\nu$(CN), upon incorporation of two charges of 34 cm^{-1}, a variation that is similar to that found in the conversion from the neutral to the anion radical of the thienoquinoidal trimers. In agreement with the above discussion, this comparison corroborates the localization of the charge in the environment of one dicyanomethylene group of the molecule in the monocharged trimers being a localized structure with one charge on one terminal group similar to that of the dianion of **B2-6TQ** which features one charge at one terminal group.

Finally, **B2-6TQ** can be oxidized to the radical cation and dication in two reversible one-electron oxidation processes. The formation of these two species has been followed by UV-Vis-NIR spectroelectrochemistry in Fig. 10 as well. The formation of the radical cation gives way to the appearance of a new strong and narrow band at 1137 nm together with a new weak component at 2204 nm. Contrarily to the formation of a radical cation in the homologue thienoquinoidal trimers (*i.e.*, formed by oxidation of a closed shell structure), oxidation of **B2-6TQ** proceeds through electron extraction in a pseudo-aromatic thienyl core (aromatization generated by diradical stabilization). This radical cation can be stabilized in two different forms, either as a quartet ground electronic state (three unpaired electrons, two unpaired electrons already in the neutral plus one more upon oxidation) or as a ground state doublet (one unpaired electron, the other two being paired), as described in Scheme 5. The relative stability of

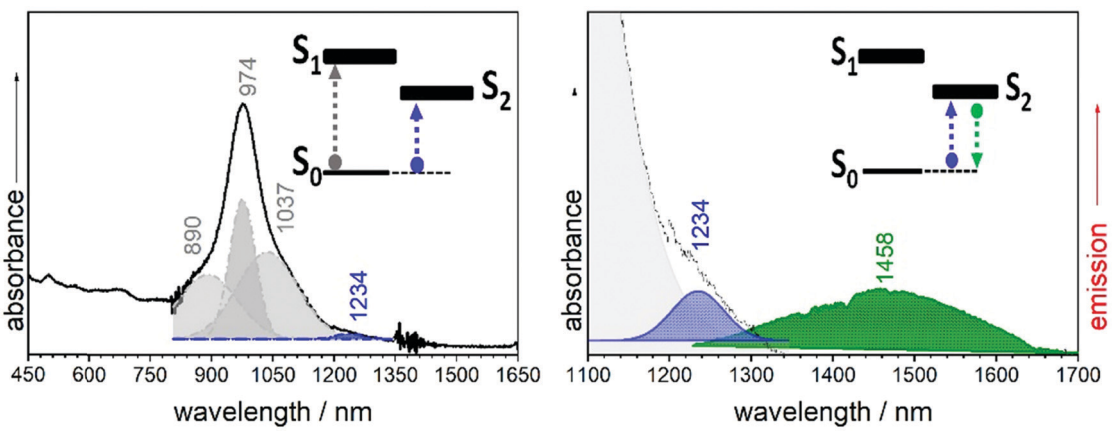

Fig. 9 Left: UV-Vis-NIR absorption spectrum (black line) of **B2-6TQ** with its deconvoluted components (grey and blue shaded). Right: 1064 nm emission spectrum (green shaded) of **B2-6TQ** at room temperature.

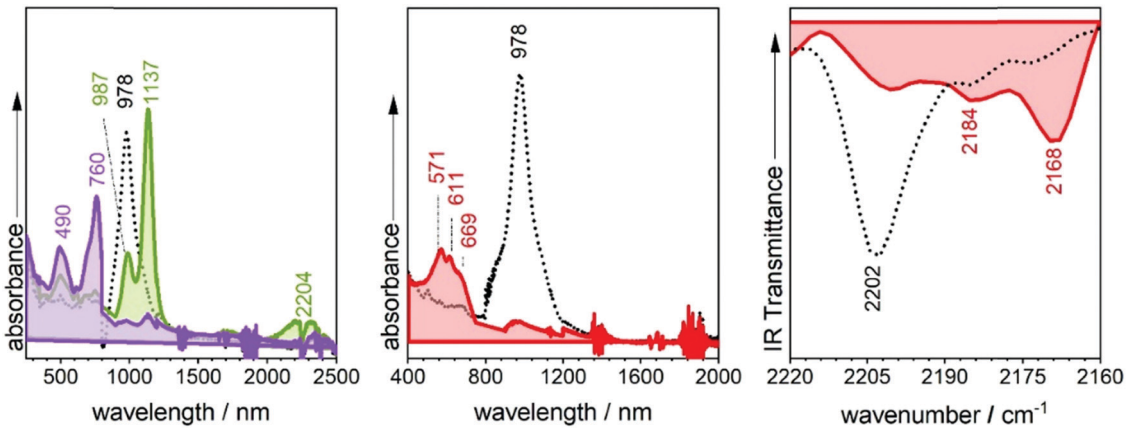

Fig. 10 UV-Vis-NIR electronic absorption spectra of **B2-6TQ** taken during the spectroelectrochemical oxidation (left, radical cation green shaded and dication purple shaded) and reduction (middle, dianion red shaded) in 0.1 M $TBPF_6$ in CH_2Cl_2 at room temperature, together with the infrared spectra of **B2-6TQ** (right, dianion, red shaded) taken under the same spectroelectrochemical reduction conditions.

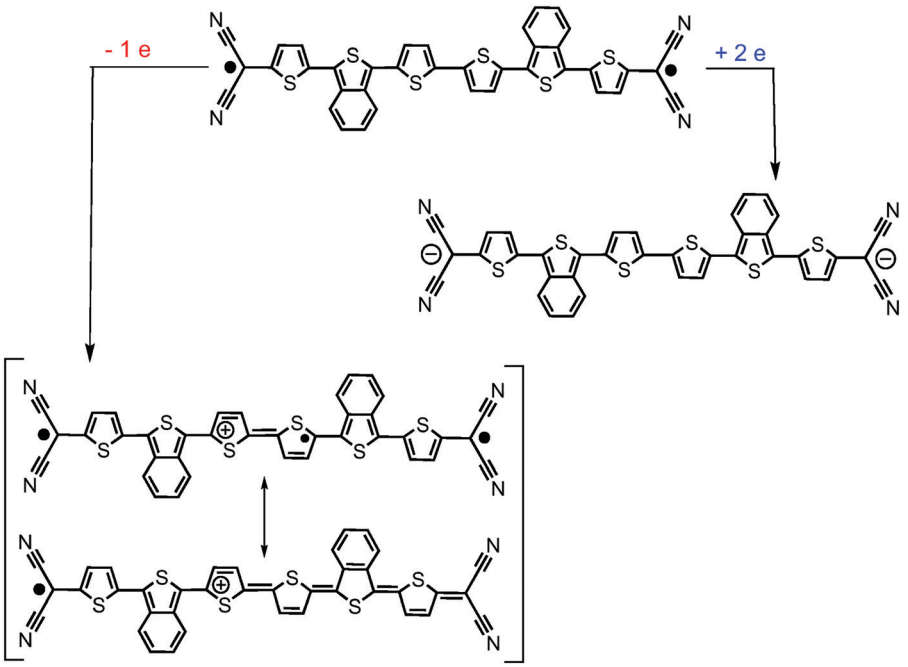

Scheme 5 Representation of the evolution of the **B2-6TQ** structure upon reduction/oxidation and upon formation of the radical cation (transiting between a triradical or a radical form).

these configurations for the radical cation of **B2-6TQ** has been explored by quantum chemical calculations in Fig. 8.

It is observed that the radical cations of the smaller tetracyanoquinoidal compounds with closed-shell structures in the neutral state disclose a doublet ground electronic state generated upon electron extraction from the doubly occupied HOMO orbital (*i.e.*, data are analyzed up to heptamers) with a first quartet high spin state always at very high energies. The energy difference between the doublet and the quartet excited state is progressively decreasing displaying a saturation effect already for the longer oligomers. The objective of this analysis was to explore the possibility to find a situation of HOMO–SOMO energy level inversion in the neutral compounds. The existence of neutral radical molecules showing HOMO–SOMO energy inversion[53,54] is now of relevance as it has been shown that these electronic configurations produce a series of benefits in the application in organic electronic devices. In the case of the neutral radical molecules, a manifestation of the SOMO–HOMO energy inversion is that oxidation of the neutral radical produces a triplet ground electronic state. In the attempt to investigate this behavior in neutral diradicals (such as **B2-6TQ**), we inspect the stabilization of the quartet ground electronic state in the oxidized radical cations as a way to confirm the SOMO–HOMO inversion effect in the starting neutral diradicals. As shown in Fig. 8, the doublet configuration is always the preferred configuration of the radical cations of the whole quinoidal series; hence, the newly

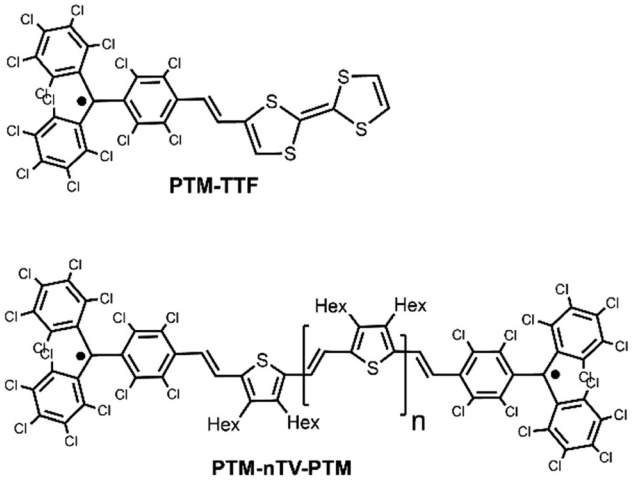

Scheme 6 Chemical structures of the Veciana and Rovira compounds with diradical character (**PTM-*n*TV-PTM**, with n = 1–6) and the PTM tetrathiafulvalene neutral radical, **PTM-TTF**.

generated radical, despite being stabilized in the central part of the molecule, ferromagnetically interacts with the radicals at both sides. In principle, the enlargement of the central thiophenic spine does not produce the doublet → quartet reversal (*i.e.*, such as it would be expected for SOMO–HOMO inversion in the neutral) and, as stated, the behavior tends towards a saturation effect. The same study, as a reference, has been done for the radical anions, and Fig. 8 also discloses the energy differences between the doublet and quartet configurations. In the two series of radical anions analyzed, the stabilization of the doublet state regarding the quartet one is larger than for the same states in the series of radical cations.

III.5. Comparison with Veciana and Rovira contributions

These π-conjugated molecules refer to several systems reported by Veciana and Rovira's group based on *para*-substituted thiophene-vinylene cores functionalized with perchlorinated triphenylene methanes (*i.e.*, PTM), as displayed in Scheme 6.[55–57]

The analogies with our studied compounds rely on their thiophenic nature, on the diradical character and on the stabilization of the radical centers by surrounding them with electron acceptor groups. **PTM-*n*TV-PTM** compounds display reversible reductions to the radical anion and dianion. In the case of the monovalent species, these are formally mixed valence systems which are reported to be class III delocalized systems in the case of **PTM-1TV-PTM** and **PTM-2TV-PTM** whereas for **PTM-4TV-PTM** and longer, all are class II/I localized mixed valence systems. There is a correlation between the behavior of **B2-6TQ** and that of the longer PTM derivatives: (i) both disclose diradical characters in the neutral state and give rise to localized radical anion systems. And (ii) the longer **PTM-*n*TV-PTM** compounds also display reversible electron oxidations, such as for example **B2-6TQ**, and give rise to doublet ground electronic states due to coupling of the thiophene-centered radical cation with those unpaired electrons in the PTM terminals. Contrarily to these cases, the **PTM-TTF** neutral radical does display SOMO–HOMO inversion (yielding triplet species upon one electron oxidation), a situation that is evaded in the medium-large size elements of the quinoidal diradicals and in the **PTM-*n*TV-PTM** compounds.

IV. Conclusions

In this paper, tetracyano thienoquinoidal compounds of different sizes and chemical compositions have been studied, and their features have been understood in the context of the properties of the well-known oligoenes (in the case of the neutral quinoidal compounds) and of the behavior of cyanines (in the case of the charged anionic states). The optical properties of these compounds in the neutral state are controlled by the energy proximity and relative energy disposition of the bright (electric dipole–dipole allowed) and dark (electric dipole–dipole forbidden) singlet excited states. Interestingly, the emission features of the quinoidal oligothiophenes fall in the near infrared spectral region which is an uncommon finding in organic molecules for NIR emitters. In the anionic state, the trimeric compounds disclose behaviors compatible with being either charge localized or delocalized mixed valence systems and can be catalogued as systems in the transition region between these two regimes of charge distribution.

The hexamer compound discloses incipient diradical character which permits the detection of the NIR emission at energies well below 1 eV. While benzoannulation of the thiophene modulates the diradical character, in parallel, it forces the confinement of the charge in the vicinity of the terminal dicyanomethylenes in the radical anions and dianions having these charge localized character. The oxidized species of the hexamer correspond with systems with charge localization in the molecular center. In the radical cation, electron extraction generates another radical in the molecular core which together with the flanking radicals (*i.e.*, already present in the neutral species) composes a triradical state which is proven to have a doublet ground electronic state. We show that by increasing the diradical character of the starting neutrals, the doublet–quartet energy gap in the radical cations is reduced but this gap is not reversed among the studied compounds.

This paper represents a research study based on spectroscopic data oriented to the elucidation of the electronic structure of organic quinoidal π-conjugated molecules of interest in organic electronic applications and in materials chemistry. The aspects of the electronic structure of the reduced species of quinoidal thienoquinoidal compounds revealed in this article might be of relevance to direct future chemical designs for n-channel organic field effect transistors and related devices.

Conflicts of interest

There are no conflicts to declare.

Acknowledgements

The authors thank the Spanish Ministry of Science, Innovation and Universities MCIU (PGC2018-098533-B-100 and RED2018-102815-T),

and the Junta de Andalucía, Spain (UMA18FEDERJA057). We also thank the Research Central Services (SCAI) of the University of Málaga.

Notes and references

1 (*a*) A. Mishra, C. Q. Ma and P. Bäuerle, *Chem. Rev.*, 2009, **109**, 1141; (*b*) I. F. Perepichka and D. F. Perepichka, *Handbook of Thiophene-based Materials*, Wiley VCH, Weinheim, 2009.
2 N. S. Zhang, B. P. Colella, S. C. Cherniawski, B. Mannsfeld and A. L. Briseno, *ACS Appl. Mater. Interfaces*, 2014, **6**, 5327.
3 H. E. Katz, L. Torsi and A. Dodabalapur, *Chem. Mater.*, 1995, **7**, 2235; A. Dodabalapur, L. Torsi and H. E. Katz, *Science*, 1995, **268**, 270.
4 C. D. Dimitrakopoulos and P. R. L. Malenfant, *Adv. Mater.*, 2002, **14**, 99; H. Sirringhaus, *Adv. Mater.*, 2014, **26**, 1319.
5 K. Schulten and M. Karplus, *Chem. Phys. Lett.*, 1972, **14**, 305.
6 M. B. Smith and J. Michl, *Chem. Rev.*, 2010, **110**, 6891.
7 D. Casanova, *Chem. Rev.*, 2018, **118**, 7164.
8 T. Takahashi, K. Matsuoka, K. Takimiya, T. Otsubo and Y. Aso, *J. Am. Chem. Soc.*, 2005, **127**, 8928.
9 S. Di Motta, F. Negri, D. Fazzi, C. Castiglioni and E. V. Canesi, *J. Phys. Chem. Lett.*, 2011, **1**, 3334.
10 L. Ren, F. Liu, X. Shen, C. Zhang, Y. Yi and X. Zhu, *J. Am. Chem. Soc.*, 2015, **137**, 11294.
11 C. Zhang and X. Zhu, *Adv. Funct. Mater.*, 2020, **30**, 765.
12 J. E. Raymond, J. Casado, J. T. Lopez Navarrete, K. Takimiya and T. Goodson III, *J. Phys. Chem. Lett.*, 2011, **2**, 2179.
13 O. Varnavski, N. Abeyasinghe, J. Arago, J. J. Serrano-Perez, E. Orti, J. T. Lopez-Navarrete, K. Takimiya, D. Casanova, J. Casado and T. Goodson III, High Yield Ultrafast Intramolecular Singlet Exciton Fission in a Quinoidal Bithiophene, *J. Phys. Chem. Lett.*, 2015, **6**, 1375–1384.
14 K. H. Kim, B. Keller, R. Ho-Wu, N. Abeyasinghe, R. J. Vázquez, T. Goodson III and P. M. Zimmerman, *J. Am. Chem. Soc.*, 2018, **140**, 7760.
15 J. Casado, L. L. Miller, K. T. R. Mann, T. M. Pappenfus, H. Higuchi, E. Ortí, B. Milián, R. Pou-Amérigo, V. Hernández and J. T. López Navarrete, *J. Am. Chem. Soc.*, 2002, **124**, 12380.
16 R. P. Ortiz, J. Casado, S. R. González, V. Holín, J. T. López-Navarrete, M. Viruela, E. Ortí, K. Takimiya and T. Otsubo, *Chem. – Eur. J.*, 2010, **16**, 470.
17 Y. Suzuki, E. Miyazaki and K. Takimiya, *J. Am. Chem. Soc.*, 2010, **132**, 10453.
18 J. C. Ribierre, S. Watanabe, M. Matsumoto, T. Muto, D. Hashizume and T. Aoyama, *J. Phys. Chem. C*, 2011, **115**, 20703.
19 D. Yuan, D. Huang, S. Medina Rivero, A. Carreras, C. Zhang, Y. Zou, X. Jiao, C. R. McNeill, X. Zhu, C. Di, D. Zhu, D. Casanova and J. Casado, *Chem*, 2019, **5**, 964–976.
20 T. Izumi, S. Kobashi, K. Takimiya, Y. Aso and T. Otsubo, *J. Am. Chem. Soc.*, 2003, **125**, 5286.
21 S. Sanvito, *Chem. Soc. Rev.*, 2011, **40**, 3336.
22 Y. Zheng, M. Miao, G. Dantelle, N. D. Eisenmenger, G. Wu, I. Yavuz, M. L. Chabinyc, K. N. Houk and F. Wudl, *Adv. Mater.*, 2015, **27**, 1718.
23 R. Kishi, Y. Murata, M. Saito, K. Morita, M. Abe and M. Nakano, *J. Phys. Chem. A*, 2014, **118**, 10837.
24 R. Kishi, M. Dennis, K. Fukuda, Y. Murata, K. Morita, H. Uenaka and M. Nakano, *J. Phys. Chem. C*, 2013, **117**, 21498.
25 K. Yamamoto, Y. Ie, M. Nitani, N. Tohnai, F. Kakiuchi, K. Zhang, W. Pisula, K. Asadi, P. W. M. Blom and Y. Aso, *J. Mater. Chem. C*, 2018, **6**, 7493.
26 K. Yamamoto, S. Jinnai, T. Takehara, T. Suzuki and Y. Ie, *Org. Lett.*, 2020, **22**, 547.
27 M. J. Frisch, G. W. Trucks, H. B. Schlegel, G. E. Scuseria, M. A. Robb, J. R. Cheeseman, G. Scalmani, V. Barone, G. A. Petersson, H. Nakatsuji, X. Li, M. Caricato, A. V. Marenich, J. Bloino, B. G. Janesko, R. Gomperts, B. Mennucci, H. P. Hratchian, J. V. Ortiz, A. F. Izmaylov, J. L. Sonnenberg, D. Williams-Young, F. Ding, F. Lipparini, F. Egidi, J. Goings, B. Peng, A. Petrone, T. Henderson, D. Ranasinghe, V. G. Zakrzewski, J. Gao, N. Rega, G. Zheng, W. Liang, M. Hada, M. Ehara, K. Toyota, R. Fukuda, J. Hasegawa, M. Ishida, T. Nakajima, Y. Honda, O. Kitao, H. Nakai, T. Vreven, K. Throssell, J. A. Montgomery, Jr., J. E. Peralta, F. Ogliaro, M. J. Bearpark, J. J. Heyd, E. N. Brothers, K. N. Kudin, V. N. Staroverov, T. A. Keith, R. Kobayashi, J. Normand, K. Raghavachari, A. P. Rendell, J. C. Burant, S. S. Iyengar, J. Tomasi, M. Cossi, J. M. Millam, M. Klene, C. Adamo, R. Cammi, J. W. Ochterski, R. L. Martin, K. Morokuma, O. Farkas, J. B. Foresman and D. J. Fox, *Gaussian 16, Revision B.01*, Gaussian, Inc., Wallingford CT, 2016.
28 A. D. Becke, *J. Chem. Phys.*, 1993, **98**, 1372.
29 M. M. Francl, W. J. Pietro, W. J. Hehre, J. S. Binkley, M. S. Gordon, D. J. Defrees and J. A. Pople, *J. Chem. Phys.*, 1982, **77**, 3654.
30 E. Runge and E. K. U. Gross, *Phys. Rev. Lett.*, 1984, **52**, 997.
31 H. H. Heinze, A. Gorling and N. Rosch, *J. Chem. Phys.*, 2000, **113**, 2088.
32 M. B. Robin and P. Day, *Mixed Valence Chemistry. A survey and classification*, Academic Press, 1968, vol. 10, p. 247.
33 N. S. Hush, *Coord. Chem. Rev.*, 1985, **64**, 135.
34 A. Heckmann and C. Lambert, *Angew. Chem., Int. Ed.*, 2012, **51**, 326.
35 J. S. Miller, *Angew. Chem., Int. Ed.*, 2006, **45**, 2508.
36 E. E. Havinga, J. L. van Donger, R. A. J. Janssen, J. Cornil and J.-L. Brédas, *Chem. – Eur. J.*, 1998, **4**, 1509.
37 J. L. Bredas and G. B. Street, *Acc. Chem. Res.*, 1985, **18**(10), 309.
38 K. Yui, H. Ishida, Y. Aso, T. Otsubo, F. Ogura, A. Kawamoto and J. Tanaka, *Bull. Chem. Soc. Jpn.*, 1989, **62**, 1547.
39 J. S. Chappell, A. N. Bloch, W. A. Bryden, M. Maxfield, T. O. Poehler and D. O. Cowan, *J. Am. Chem. Soc.*, 1981, **103**, 2442.
40 S. Ohira, J. M. Hales, K. J. Thorley, H. L. Anderson-Joseph, W. Perry and J. L. Brédas, *J. Am. Chem. Soc.*, 2009, **131**, 6099.
41 P. A. Bouit, C. Aronica, L. C. Toupet, B. Le Guennic, C. Andraud and O. Maury, *J. Am. Chem. Soc.*, 2010, **132**, 4328.
42 L. M. Tolbert and X. Zhao, *J. Am. Chem. Soc.*, 1997, **119**, 3253.
43 F. Würthner, *Angew. Chem., Int. Ed.*, 2020, **59**, 14192.
44 J. L. Zafra, L. Qiu, N. Yanai, T. Mori, M. Nakano, M. P. Alvarez, J. T. López Navarrete, C. J. Gómez-García, M. Kertesz,

K. Takimiya and J. Casado, *Angew. Chem., Int. Ed.*, 2016, **55**, 14563.
45 L. L. Miller and K. R. Mann, *Acc. Chem. Res.*, 1996, **29**, 417.
46 J. C. Evans, A. G. Evans, N. H. Nouri-Sorkhabi, A. Y. Obaid and C. C. Rowlands, *J. Chem. Soc., Perkin Trans. 2*, 1985, 315–318.
47 D. D. Graf, J. P. Campbell, L. L. Miller and K. R. Mann, *J. Am. Chem. Soc.*, 1996, **118**, 5480.
48 A. Harbuzaru, I. Arrechea-Marcos, A. D. Scaccabarozzi, Y. Wang, X. Guo, M. Caironi, J. T. López-Navarrete, M. C. R. Delgado and R. P. Ortiz, *J. Mater. Chem. C*, 2020, **8**, 15759.
49 J. S. Miller and J. J. Novoa, *Acc. Chem. Res.*, 2007, **40**, 189.
50 J. J. Novoa, P. Lafuente, R. E. D. Sesto and J. S. Miller, *Angew. Chem., Int. Ed.*, 2001, **113**, 2608.
51 J. Casado, P. Mayorga Burrezo, F. J. Ramírez, J. T. López Navarrete, S. H. Lapidus, P. W. Stephens, H. L. Vo, J. S. Miller, F. Mota and J. J. Novoa, *Angew. Chem., Int. Ed.*, 2013, **52**, 6421.
52 K. Yamaguchi, *Chem. Phys. Lett.*, 1975, **33**, 330.
53 Y. Wang, H. Zhang, M. Pink, A. Olankitwanit, S. Rajca and A. Rajca, *J. Am. Chem. Soc.*, 2016, **138**, 7298.
54 A. Abdurahman, T. J. H. Hele, Q. Gu, J. Zhang, Q. Peng, M. Zhang, R. H. Friend, F. Li and E. W. Evans, *Nat. Mater.*, 2020, **19**, 1224.
55 C. Franco, P. M. Burrezo, V. Lloveras, R. Caballero, I. Alcón, S. T. Bromley, M. Mas-Torrent, F. Langa, J. T. López-Navarrete, C. Rovira, J. Casado and J. Veciana, *J. Am. Chem. Soc.*, 2017, **139**(2), 686.
56 J. Guasch, L. Grisanti, V. Lloveras, J. Vidal-Gancedo, M. Souto, D. C. Morales, M. Vilaseca, C. Sissa, A. Painelli, I. Ratera, C. Rovira and J. Veciana, *Angew. Chem., Int. Ed.*, 2012, **51**, 11024.
57 M. Souto, J. Guasch, V. Lloveras, P. Mayorga, J. T. Lopez-Navarrete, J. Casado, I. Ratera, C. Rovira, A. Painelli and J. Veciana, *J. Phys. Chem. Lett.*, 2013, **4**, 2721.